Journal of the European Ceramic Society 44 (2024) 116648

Contents lists available at ScienceDirect

Journal of the European Ceramic Society

journal homepage: www.elsevier.com/locate/jeurceramsoc

Atom probe tomography investigation of sintered transition metal carbonitride - A Zr(C,N) study

Idriss El Azhari [a,*], Jenifer Barrirero [a], José García [b], Christoph Pauly [a], Frank Mücklich [a]

[a] Chair of Functional Materials, Department of Materials Science, Saarland University, Campus D 3.3, Saarbrücken D-66123, Germany
[b] AB Sandvik Coromant R&D Lerkrogsvägen 19, Stockholm SE-126 80, Sweden

ARTICLE INFO

Keywords:
Zirconium carbide ZrC
Zirconium nitride ZrN
Stoichiometry
Hard material
APT

ABSTRACT

Zirconium based nitrides, carbides and carbonitrides are highly technological compounds which received during the 1950s and 60s huge interest due to their combination of metal and refractory properties. The interest reiterated recently due to the need of compounds with high electrical conductivity, corrosion and oxidation resistance, and neutron transparency with the rise of mobility electrification and nuclear energy. Sintered Zr(C,N) is investigated with CHN elemental analysis combined with atom probe tomography (APT) to evaluate the composition and homogeneity of carbon and nitrogen from the bulk down to the nanometer scale. Results have shown a strong nitrogen loss and an enrichment in carbon which diffused from the graphite die and punch. Nevertheless, the composition is homogenous in the sample. Atom probe tomography suggests that the sintered alloy is sub-stoichiometric with carbon and nitrogen homogeneously distributed within the grain. The stoichiometry calculated corresponds to the estimation by Vegard's law.

1. Introduction

Zirconium carbides, nitrides and their quasi-binary solid solutions (carbonitrides) are crystalline alloys with FCC (B1) structure in which carbon and/or nitrogen take the octahedral interstices [1]. They belong to the Group VI transition metal compounds combining ceramic and metallic properties thanks to their complex electronic configuration. These zirconium alloys are particularly interesting due to their very high melting temperature (Ultra High Temperature Ceramics) [2,3], high electrical conductivity, corrosion resistance, low neutron absorption, low coefficient of friction, bio-compatibility [4,5], and tribological properties. Accordingly, it attracts a growing interest in many key technological applications: micro-electronics [6], nuclear and fusion reactors [7,8], energy production and conversion [9,10] and for cutting tools either as wear resistant thin coatings [11–14] or as gamma-phase forming elements in cemented carbides to enhance mechanical properties at highspeed machining [15]. These compounds are mainly produced and studied as thin films through vapor deposition routes (Chemical Vapor Deposition (CVD), Physical Vapor Deposition (PVD)) or in bulk form through compaction and sintering of carbonitride powder. It was reported that the mixing of carbides and nitrides is a possible route to produce single phase Zr(C,N) [16,17], which requires very high pressure and temperature for the diffusion of carbon and nitrogen. The literature on Zr(C,N) as thin films is not rich as it is for ZrC and ZrN. When it comes to sintered Zr(C,N) alloys, to the best knowledge of the authors, the only bibliography available is that from Harrison et al. [18–20] and earlier reports from the 60's and 70's [16,17,21]. Generally, for these alloys produced with powder metallurgy methods, many of the reports suffer from a lack of rigorous characterization of the chemistry, its microstructure or both. Precise data on chemical composition and impurities are known to directly influence the reported properties of these compounds. Physical and mechanical properties of transition metal carbonitrides depend on the C/N ratio, which makes determination and control of carbon and nitrogen concentrations and vacancies key factors for tailoring properties of these compounds [22,23]. It was even stated that the stoichiometric composition of ZrCxOyNz is considered as one of the most important issues regarding the synthesis and applications [24]. Nevertheless, precisely determining the composition of the light elements (carbon, nitrogen and oxygen) for the carbonitrides is quite challenging. In the present work, chemical

* Corresponding author.
E-mail address: idriss.elazhari@uni-saarland.de (I. El Azhari).

https://doi.org/10.1016/j.jeurceramsoc.2024.05.070
Received 20 March 2024; Received in revised form 15 May 2024; Accepted 28 May 2024
Available online 28 May 2024

composition, homogeneity and stoichiometry of a sintered Zr(C,N) alloy is measured using energy-dispersive X-ray spectroscopy (EDS), CHN elemental analysis and atom probe tomography (APT). The main objectives are: (1) the investigation of the chemical homogeneity (potential composition variations) in the bulk and on the micrometer scale, (2) the comparison of the composition variations between the initial powder and the sintered bulk alloy, especially the C/N ratios, and finally (3) the characterization of the composition and stoichiometry with high accuracy.

2. Experimental part

2.1. Sample production

Zr(C0.5,N0.5) commercial powder (1.3 μm, Zr: 86.4 wt%, C: 5.6 wt %, N: 6.7 wt%, O: 0.4 wt%; A.L.M.T., SUMITOMO Group, Japan) is used to produce Zr(C,N) bulk samples. The powder is consolidated in a hot press by uniaxial pressing. Zr(C,N) powder is placed in a graphite die between two graphite punches (Fig. 1(a)). The graphite set-up is placed in the hot press furnace. The furnace is closed and filled with argon (Ar), then the Ar is pumped out to remove impurities from the furnace atmosphere until a pressure of 10 mbar is reached. Then the sintering process is set to two stages by heating up then holding the temperature at 1500°C and 2000 °C with a heating rate of 5 °C/min (Fig. 1(b)). Uniaxial pressure is applied also at two stages. Once the high temperature is reached, a pressure of 200 bar is applied for 1 h to densify the powder. Afterwards, the cooling ramp at a rate of 10 °C/min is set until reaching room temperature. The sample is then removed from the graphite crucible and grinded on all sides to remove the graphite adhered to the sintered piece. The sample has the shape of a pellet with a diameter of 20 mm. A density > 96% is achieved by the hot press process described above. Lattice parameters of the sintered sample were determined using X-ray diffraction (XRD) in a PANalytical X'pert PRO MPD with filtered Cu-Ka radiation in the 2θ range of 30–145° in Bragg-Brentano geometry. Pattern analysis and refinement (Pawley method) was done with PANalytical Highscore software. For microscopy analysis the sample was grinded and polished to have mirror finished surface. The last polishing step was done with alumina suspension (OP-A, Struers).

2.2. EDS analysis

Energy Dispersive X-ray Spectroscopy was carried out with an EDAX detector installed in a FEI Helios NanoLab 600 DualBeam FIB/SEM and in a Thermo-Fisher Helios G4 PFIB CXe DualBeam FIB/SEM. The objective is to have an overview of the chemical elements existing in the sample and a rough quantification. 5–10 kV acceleration voltage is used. Approximate quantification is done after peak fitting and background subtraction using ZAF method. C and N quantification are performed without a standard as the goal is to have an estimation of the composition which will be compared afterwards with the CHN and APT elemental analyses. EDS was used together with SEM to analyze the composition of the different phases/components and their spatial distribution in the sintered ceramic.

2.3. Atom probe tomography

Atom probe tomography was performed to measure the chemical composition of the sintered materials with high resolution, mainly the C/N ratio (that will be compared to the powder base composition) and quantify contamination and trace elements. Additionally, this technique can give an insight into the homogeneity of the composition or potential presence of clustering due to high temperature and pressure during sintering. APT specimens were prepared so that the long axis of the reconstruction is perpendicular to the surface of the material. Samples were prepared in a dual-beam FIB/SEM workstation (FEI Helios NanoLab 600) by using the lift-out technique described by Thompson et al. [25]. After thinning, a low energy milling at 2 kV was performed to minimize gallium contamination. APT was carried out in a LEAP 3000X HR (CAMECA) in voltage mode with 20% pulse fraction. All measurements were performed at repetition rate of 200 kHz, pressure lower than 1.33×10^{-8} Pa, evaporation rate of 1 atom per 200 pulses and a specimen temperature between 60 and 70 K. Datasets were reconstructed and analyzed with IVAS™3.6.8 software (CAMECA).

2.4. CHN analysis

CHN chemical analysis method was used to analyze the bulk composition in terms of C/N fraction with larger sampling volume than APT. The method relies on high temperature decomposition of the sample through combustion in an oxygen/helium environment, then the separation and chemical analysis of the resulting gases. Vario Micro Cube analyzer (Elementar GmbH, Germany) is used with an amount not exceeding 5 mg of the sample for the analysis (with an accuracy of $\pm10^{-3}$ mg). Considering that the volume analyzed by APT is in the range of 1.6×10^{-12} mm^3 (80 nm × 80 nm × 250 nm), the volume analyzed with CHN method is around 10^{11} larger.

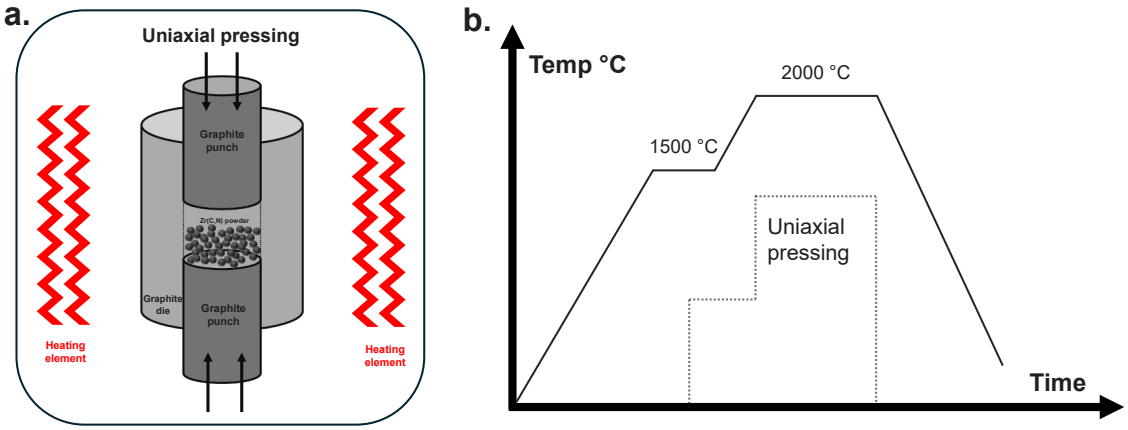

Fig. 1. a. Schematic of hot pressing of Zr(C,N) powder showing the graphite punch and die. The gas pressure is maintained at 10 mbar of argon. b. Temperature and uniaxial pressure profile evolution with time during sintering.

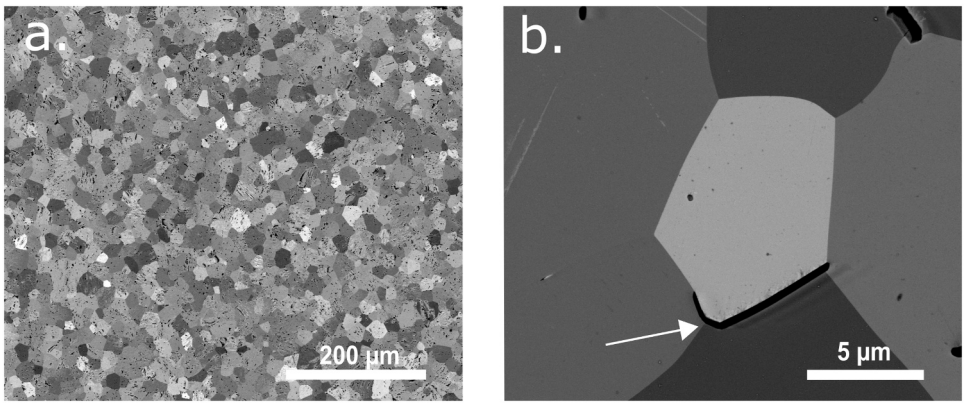

Fig. 2. a. Equiaxed microstructure of the sample imaged with backscattered electrons. b. White arrow shows dark inclusions present in the sample.

3. Results and discussion

3.1. Metallography

Fig. 2 shows equiaxed grain shape with different orientations as evident from the strong orientation contrast in the backscattered SEM image. Porosity is seen across the entire sample; dark inclusions are found as seen in Fig. 2(b). Thorough investigation and insights on the microstructure will be given in a separate communication. The inclusions are further analyzed with EDS.

3.2. EDS analysis

EDS spectra gives a preview of elements in the sample, in addition to the main expected elements (zirconium, carbon and nitrogen), oxygen and hafnium are also found with small amounts. The black inclusions were analyzed and compared locally to the surrounding material in Fig. 3. It is clearly depicted that the inclusions are formed of almost pure carbon. Very small peaks of other elements such as Zr L and O K are probably caused by the X-ray interaction volume exceeding the carbon phase due to its small dimensions. For a rough estimation of the composition in a larger area, a standardless quantification of the elements present in the alloy at 10 kV acceleration voltage is given in Table 1. Traces of aluminum and slightly higher oxygen composition could come from contamination/residues using alumina suspension as the final polishing step. It is seen that we have an increase of carbon and a strong drop in nitrogen content.

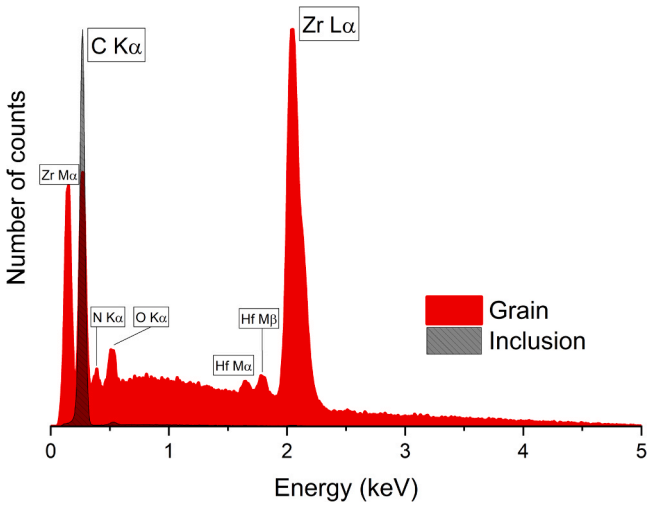

Fig. 3. Comparison of EDS spectrum (with rescaling of the inclusion spectra) between dark inclusions (grey filled curve) and the Zr(C,N) grain (red filled curve) measured at 5 kV acceleration voltage.

Table 1
Standardless EDS quantification at 10 kV acceleration voltage of chemical elements present in the sintered alloy using ZAF method. The values are compared with chemical composition of the used Zr(C,N) powders. NB: Quantification for light elements with small amounts is not accurate. Values presented in the table are indicative.

	EDS of sintered alloy		Nominal powder composition
	at%	wt%	wt%
Zr	54.8	87.3	86.4
C	38.8	8.1	5.6
N	3.5	0.9	6.7
O	1.6	0.5	0.4
Hf	1	3.1	-
Al	0.3	0.1	-

3.3. APT

APT analysis of carbides, nitrides and carbonitrides have been performed almost exclusively using laser pulse evaporation [26–33]. Voltage pulsing mode for these compounds is possible when they are analyzed in form of precipitation inside a metal matrix [34–39], although even in that case laser mode is sometimes used [40]. Laser pulse evaporation uses a thermal activation, and thermal tails often accompany the peaks in the mass spectrum used for the compositional quantification. Thermal tails can be of disadvantage, since small peaks can be lost below the tail of a larger peak and the ranging of peaks with large tails is a challenging task [41,42]. Measuring in voltage mode, on the contrary, can result in sharper peaks increasing mass resolution. Early works in the 1980s and 90s, showed the use of voltage mode in APT and Atom Probe Field Ion Microscopy (APFIM) for WC [43–45].The limitation of voltage pulsed evaporation is that the material should be electrically conductive, and the specimen thinned to a sharp tip to evaporate within the range of voltage available for the measurement (up to about 11–13 kV), which can result in an early specimen fracture. In comparison to traditional ceramics, zirconium carbides and nitrides are excellent conductors with a resistivity as low as that of the zirconium metal [1,46]. For this reason, in the present study voltage mode has been used on a Zr(C,N) sample, getting successful measurements.

Two reconstructions with 24 and 42 million detected counts are considered in this work. Both reconstructions showed a homogeneous distribution of the elements with no clustering present in the material. Fig. 4(a–c) show an example of the distribution of Zr, N, and C together with a concentration profile depicting a constant concentration evolution of the main elements during measurement. The calculation of the compositions reported in Table 2 were obtained by considering the counts in cylindrical regions of interest with 8.6 million ranged counts (diameter: 50 nm; length: 200 nm) (Fig. 4(a)) and 16.6 million ranged

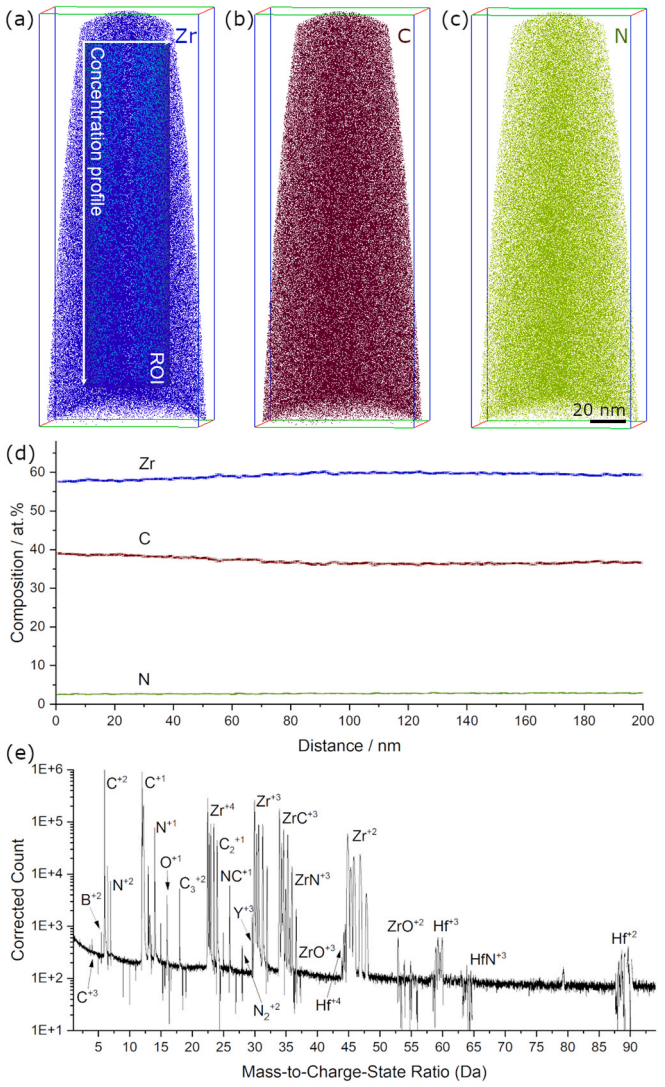

Fig. 4. APT reconstruction of a specimen in the Zr(C,N) grain. (a-c) Homogeneous elemental distribution of Zr, C and N. Representation of the cylindrical ROI used for the concentration profile and the calculation of the composition. (d) Concentration profile along the reconstruction showing a stable composition evolution. (e) Mass spectrum.

counts (diameter: 80 nm; length: 170 nm) to avoid the border of the reconstruction. These measurements were performed at two different sample temperatures (60 K and 70 K) to test the stability of the measurements and the difference in the acquisition quality. The change in temperature showed a clear change in the amount of single hits. The measurement performed at 60 K showed a slightly lower background, however, the amount of single hits was limited to about 40%. In contrast, the measurement performed at 70 K, presented 60% singles with a slightly higher background. Nitrides and carbonitrides are known to show a high amount of multiple hit events during APT measurements [26,28–30,47]. To control and correct for potential losses of carbon due to the presence of multiple hit events, the ^{13}C-method presented in literature was applied [47]. However, the isotopic ratios of C^{+} and C^{+2} where as expected, giving the indication that there was no loss on these peaks, which are the largest peaks of carbon in the measurements. Alongside, a peak decomposition analysis was performed to resolve overlapping peaks in two regions of the spectrum. One of the overlaps is found for ZrC^{+3} / ZrN^{+3} / ZrO^{+3} in the range between 34 and 37 Da. In this case, the overlap can be easily solved, because each of the compounds has 8–9 isotopes with some peaks having no overlap that can be used unambiguously for the decomposition calculation. Most of the counts in these peaks belonged to ZrC. The second overlap was found for Hf^{+4} / Zr^{+2} / Y^{+2} at 44 Da. Revising the isotopic ratios, it was confirmed that most of the peak belonged to Zr, the Hf fraction was calculated from its isotopic ratio, and no Y was present in this peak. Fig. 4(e) shows an example of a mass spectrum. Table 2 shows the composition calculated after background subtraction for both reconstructions. Despite the difference in the amount of single hits obtained during the acquisition, a consistent and reproducible composition was confirmed. Oxygen content measured with APT is lower than EDS results as the sampling is done by lift-out from below the sample surface in contrast to EDS which is performed on the surface.

Table 2
APT composition comparison of the two reconstrcutions performed at 70 and 60 K, respectively.

Elements	*Peak decomposition*	*Peak decomposition*
ROI	D = 80 nm L = 170 nm	D = 50 nm L = 200 nm
Ranged counts	16.6 M	8.6 M
Single hit events	60%	40%
Temperature	70 K	60 K
Elements	*at%*	*at%*
Zr	60.36 ± 0.02	59.85 ± 0.01
C	36.57 ± 0.01	36.64 ± 0.02
N	2.38 ± 0.01	2.49 ± 0.01
Hf	0.32 ± 0.01	0.50 ± 0.01
Ti	0.10 ± 0.01	0.19 ± 0.04
O	0.17 ± 0.01	0.24 ± 0.01
B	0.01 ± 0.01	0.02 ± 0.01
Al	0.02 ± 0.01	0.02 ± 0.01
Y	0.05 ± 0.01	0.06 ± 0.01

Table 3
Carbon and nitrogen content comparison between APT and CHN method. *The conversion of wt% to at% for the CHN method was calculated considering that Zr balances the experimentally measured C and N fractions.

	APT		**CHN**	
	at%	**wt%**	**wt%**	**at%***
Zr	60.2	90.8	-	52.1*
C	36.6	7.3	10.2	45.5*
N	2.4	0.6	0.6	2.4*
Hf	0.4	1.2	-	-
Ti	0.1	0.1	-	-
O	0.2	0.1	-	-
Total	100	100	-	100*

3.4. CHN analysis and composition comparison

C and N contents determined by CHN method are 10.24 ± 0.69 wt% and 0.62 ± 0.07 wt%, respectively. Comparison of the results with APT is presented in Table 3. APT weight% were calculated by conversion of atomic%.

The comparison shows that carbon is around 3 wt% higher than in APT, while the nitrogen composition is very similar for both methods. CHN method is a bulk large-scale method in comparison to APT which is a measurement in the nano-metric scale. The higher carbon fraction measured by CHN comes from the carbon flakes and inclusions which are spread across the sample. The APT specimens were taken inside a grain avoiding these inclusions which are found by EDS to be almost pure carbon. For nitrogen, the content obtained from both methods is nearly the same, meaning that the nitrogen concentration in the bulk and very locally at the microstructure level is constant and homogeneous. In the next paragraph the reasons behind variation of C/N ratio from the base powder to the sintered alloy will be discussed.

3.5. C/N ratio variations

The C/N ratio is a key parameter to tailor physical properties of these carbonitrides. Combination of the CHN method which is a bulk large-scale method with the APT method that measures chemistry at the atomic scale is complementary and insightful. Both methods have given a similar result regarding the nitrogen content in the material which was considerably reduced in the sintering process from the base powder. In comparison with the composition of the base powder, the C/N ratio changed from around 1 to 15. The main reason is nitrogen evaporation during sintering. The comparison of the results with literature reports is not straightforward, since the experimental conditions, parameters and sintering equipment differ, impacting the composition and microstructure. For example, Harrison et al. who produced Zr(C,N) from carbothermic reduction of zirconia powder have not reported a considerable loss of nitrogen [18–20], however the sintering was performed under argon pressure of 1 bar compared to the 10 mbar used in the present study. For ZrN, over-stoichiometric nitrogen content is not possible and the excess of nitrogen converts to N_2 gas as it can be seen from the phase diagram [48,49]. Additionally, it is documented that nitrogen evaporates during sintering and escapes as N_2 gas, while sintering under N_2 atmosphere reduces the nitrogen loss in the alloy. Early reports stated that ZrN releases N_2 at temperatures considerably below the melting temperature, and heating ZrN under vacuum can start releasing/evaporating nitrogen already at temperatures of 500°C [50]. It has been shown that sintering or annealing of ZrN in vacuum decreases nitrogen content to the lower limit of the homogeneity range, oppositely to sintering or post annealing in nitrogen that maintain approximately the stoichiometry [51]. Furthermore, Wheeler et al. suggested that sintering under argon increases nitrogen deficiency in comparison to sintering under nitrogen [52]. In another study, although sintered in vacuum, Alexander et al. reported no decrease in nitrogen stoichiometry (no nitrogen loss) [53]. However, the used technique is hot isostatic pressing (HIP) in which powders are pressed and sintered in silica and titanium containers [53] that may act as an hermetic seal, and no gas can escape in contrast to standard graphite die and punch used in hot pressing. From these literature results, it can be deduced that the N_2 vapor pressure during sintering plays a key role in preventing nitrogen loss from the alloy. Accordingly, nitrogen loss in this experiment is mainly attributed to sintering in dynamic vacuum environment. Even for the perfect crucible set up, the compartment inside is not sealed (i.e. not gas tight) which cannot prevent the interaction with the hot-press sintering atmosphere. To avoid the evaporation (loss of N) in the Zr(C,N) a counter-pressure of N should be applied, so that the nitrogen activity in the Zr(C,N) sample is equal to the nitrogen activity in the hot-press atmosphere. This is rather difficult in a dynamic vacuum process. Hence a loss of N during the consolidation process occurred, as confirmed experimentally.

Regarding the carbon content of the alloy, it is known that over-stoichiometric ZrC in carbon does not exist and that the exceeding carbon is segregated as graphite [54]. Carbon in the form of graphite in sintered ZrC was detected and measured by using nuclear magnetic resonance spectrometry (NMR) [55]. Even with the use of a graphite foil to prevent interaction between the powder and the graphite container, it was reported that carbon can diffuse from the foil to the sample [56]. In the present study, no intercalation between the graphite crucible setup with the powder was used which might enhance carbon diffusion to the alloy, considering that the sintering was performed at high temperatures (2000°C). The existing porosity from the compaction and grain coalescence could act as fast channels for diffusion which explains the carbon flakes and inclusions across the sample. However, APT results suggest that carbon diffused also inside the grains and fills the evaporated nitrogen interstices. Similar result of nitrogen loss and carbon enrichment was reported by Das et al. during flash sintering of ZrN [57].

3.6. Stoichiometry of the carbonitride

It has been reported that measuring precisely the stoichiometry of these compounds is challenging and not straightforward task, requiring the combination of elemental analyses with other analytical techniques for a precise determination (e.g. RAMAN, NMR, TGA) [55,56]. The estimation of the stoichiometry from APT analysis should be done with precautions knowing that a high amount of multiple hits can cause deviations in the quantification. However, since the analysis in this study presented consistent compositions for different levels of multiples, and carbon isotopic ratios corresponding to the expected isotopic ratios, it can be assumed that the measured stoichiometry corresponds closely to that of the sample. Considering this result, the composition changed from a powder composition of around $Zr(C_{0.5},N_{0.5})$ ($Zr_{0.5}(C_{0.25},N_{0.25})$) to a sintered sub-stochiometric alloy $Zr(C_{0.6},N_{0.04})$ ($Zr_{0.61}(C_{0.37},N_{0.02})$) with nitrogen loss and carbon enrichment. APT analysis showed that all three elements are homogenously distributed within the grain with no clustering of carbon or nitrogen. Existence of large number of vacancies (up to 50% vacancy) in the sub-lattice does not imply rock salt structure lattice instability [56,58]. Nevertheless, these vacancies affect the bulk properties of the zirconium compounds [59].

Measuring the lattice parameter with X-Ray diffraction is a standard method to estimate the stoichiometry of the carbides, nitrides and their combination as the lattice volume is strongly influenced by the site occupancy. However, the determination of the correlation/relationship of the lattice parameter with the stoichiometry is quite challenging and subject of debate and controversy. Carbon, nitrogen, and oxygen atoms occupying the lattice sites modify the atomic bonding and charge density in different ways. The resulting lattice volume is a complex interplay of their corresponding effects and difference of atomic diameters. For zirconium carbides, in his handbook back from the 1960s, Kieffer [60] had already raised the issue of a strong scattering of the lattice constant values reported in the literature. At that time, this was attributed to the existing impurities in the alloy [60]. Few analytical expressions were reported correlating oxycarbonitride compositions to lattice parameter, nevertheless these parametrizations are likely to be applicable within a set of samples produced from the same synthesis procedure [24]. To this day, the scattering of the values is still troublesome. Due to the complicated manufacturing of pure specimens and the application of adequate characterization methods, hence establishing a conclusive relationship is still challenging [7,55]. The known general trends imply that an increase of carbon in ZrC increases the lattice constant, while an increase of oxygen content decreases it [7,21,61]. This is explained by the modification of the bonding [61,62]. For ZrN, oppositely, it has been reported that an increase in nitrogen decreases slightly the lattice parameter [63,64], and an increase of oxygen in the lattice expands it [21]. For oxycarbonitrides, based on various literature values, Mitrokhin et al. established a quantitative correlation between lattice parameter and composition of C, O and N [65,66]:

$$a(ZrCx(O,N)y) = 4.5621 - 0.2080x^2 + 0.3418x - 0.80y(1 - x)$$

where x=C/Zr and y=(O+N)/Zr with $0.62 \leq x \leq 1$ and $y \leq 0.3$. The two possible solutions (x) for this equation when using the APT result y=0.04, and the lattice parameter determined by X-ray diffraction a=4.693 Å, are x_1=1.05 and x_2=0.75. These solutions are not consistent with the x=C/Zr=0.6 obtained by APT. In the present study, the analyzed sample shows a very low oxygen concentration (<0,1 wt%) confirming the absence of the oxycarbonitrides when taking into consideration the average oxygen boundary composition discussed in the work of Réjasse et al. [62]. This result casts doubt on the applicability of this equation when analyzing only zirconium carbonitride without the presence of oxygen.

For Zr(C,N), it was reported that the lattice constant is varying from ZrN to ZrC according to Vegard's law [16,65,67]. Considering this empirical rule proposed by Vegard [68,69] with a linear relationship

between the crystal lattice constant and the concentration of the constituent elements, and considering the stoichiometric lattice parameters of ZrC = 4.70 Å [24,46,70–72] and ZrN = 4.57 Å [22,24,70], Vegard's law is applied in the present case. A precise correspondence is found comparing the carbon proportion as given by Vegard's law, $C/(C+N)_{Vegard}$=0.9465; and the proportion obtained by APT, $C/(C+N)_{APT}$= 0.9385. The very good fit could be credited to low oxygen and absence of oxycarbonitride. This outcome confirms the stoichiometry estimation by using APT and supports the use of this analytical technique for the precise determination of the composition and stoichiometry of these compounds.

4. Conclusions

The chemical composition of a Zr(C,N) sintered alloy was investigated from bulk scale using CHN analysis and EDS down to the nanometer scale with APT. The focus was put on the analysis of the variation of the chemical composition and homogeneity after sintering. The following conclusions could be drawn:

- Atom probe tomography measurements for carbonitrides zirconium alloys can be performed using voltage pulsing mode.
- After sintering, considerable loss of nitrogen took place with a strong diffusion of carbon from the sintering graphite media (graphite punches and die) through the porosity, forming then carbon inclusions. Carbon stoichiometry inside the grain increased as well. Nevertheless, carbon and nitrogen are homogeneously distributed within single crystals.
- Carbon and nitrogen concentrations from CHN analysis and APT agreed and correlated. Chemical composition is homogeneous across the sample, N bulk composition correlates very well with localized nanometric composition.
- According to the APT results, after sintering a sub-stoichiometric alloy is formed around $Zr(C_{0.6},N_{0.04})$. This result is supported by Vegard's law for the carbonitride which correlates very well with the APT results.
- APT can be used as reliable method to measure the composition, homogeneity and stoichiometry with high accuracy.

CRediT authorship contribution statement

Frank Mücklich: Resources, Project administration, Funding acquisition, Conceptualization. **Christoph Pauly:** Writing – review & editing, Validation, Methodology, Investigation, Formal analysis, Data curation. **José Garcia:** Writing – review & editing, Validation, Supervision, Resources, Methodology, Formal analysis. **Jenifer Barrirero:** Writing – review & editing, Writing – original draft, Visualization, Validation, Methodology, Investigation, Formal analysis, Data curation, Conceptualization. **Idriss El Azhari:** Writing – review & editing, Writing – original draft, Visualization, Validation, Supervision, Project administration, Methodology, Investigation, Funding acquisition, Formal analysis, Data curation, Conceptualization.

Declaration of Competing Interest

The authors declare that they have no known competing financial interests or personal relationships that could have appeared to influence the work reported in this paper.

Acknowledgements

This work would not have been possible without the support of the German Research Foundation (DFG) within the project "Investigation of plastic deformation mechanisms and microstructural characteristics of transition metal carbonitrides, Zr(C,N) and Ti(C,N) hard coatings" (project number 496845180). The authors would like to thank Ms Susanne Harling (Chair of Inorganic Solid State Chemistry, Service points analytics, Saarland University) for performing the CHN Analysis. Sandvik Coromant is acknowledged for providing the samples for the study. Funding for the FIB/SEM instrument Helios G4 PFIB CXe by the DFG is acknowledged (project number 415217285).

References

[1] A. Ul-Hamid, Microstructure, properties and applications of Zr-carbide, Zr-nitride and Zr-carbonitride coatings: a review, Mater. Adv. 1 (2020) 1012–1037, https://doi.org/10.1039/D0MA00233J.
[2] W.G. Fahrenholtz, G.E. Hilmas, I.G. Talmy, J.A. Zaykoski, Refractory diborides of zirconium and hafnium, J. Am. Ceram. Soc. 90 (2007) 1347–1364, https://doi.org/10.1111/j.1551-2916.2007.01583.x.
[3] I.L. Shabalin, Introduction. Ultra-High Temp. Mater. II, Springer Netherlands, Dordrecht, 2019, pp. 1–8, https://doi.org/10.1007/978-94-024-1302-1_1.
[4] I. Ferreri, V. Lopes, S. Calderon V, C.J. Tavares, A. Cavaleiro, S. Carvalho, Study of the effect of the silver content on the structural and mechanical behavior of Ag–ZrCN coatings for orthopedic prostheses, Mater. Sci. Eng. C 42 (2014) 782–790, https://doi.org/10.1016/j.msec.2014.06.007.
[5] L. Wang, X. Zhao, M.H. Ding, H. Zheng, H.S. Zhang, B. Zhang, X.Q. Li, G.Y. Wu, Surface modification of biomedical AISI 316L stainless steel with zirconium carbonitride coatings, Appl. Surf. Sci. 340 (2015) 113–119, https://doi.org/10.1016/j.apsusc.2015.02.191.
[6] R. Fix, R.G. Gordon, D.M. Hoffman, Chemical vapor deposition of titanium, zirconium, and hafnium nitride thin films, Chem. Mater. 3 (1991) 1138–1148, https://doi.org/10.1021/cm00018a034.
[7] H.F. Jackson, W.E. Lee, Properties and Characteristics of ZrC. Compr. Nucl. Mater., Elsevier, 2012, pp. 339–372, https://doi.org/10.1016/B978-0-08-056033-5.00023-9.
[8] R. Liu, Z.M. Xie, J.F. Yang, T. Zhang, T. Hao, X.P. Wang, Q.F. Fang, C.S. Liu, Recent progress on the R&D of W-ZrC alloys for plasma facing components in fusion devices, Nucl. Mater. Energy 16 (2018) 191–206, https://doi.org/10.1016/j.nme.2018.07.002.
[9] J. Xu, H.J. Huang, Z. Li, S. Xu, H. Tao, P. Munroe, Z.-H. Xie, Corrosion behavior of a ZrCN coated Ti alloy with potential application as a bipolar plate for proton exchange membrane fuel cell, J. Alloys Compd. 663 (2016) 718–730, https://doi.org/10.1016/j.jallcom.2015.12.197.
[10] Y. Yuan, J. Wang, S. Adimi, H. Shen, T. Thomas, R. Ma, J.P. Attfield, M. Yang, Zirconium nitride catalysts surpass platinum for oxygen reduction, Nat. Mater. 19 (2020) 282–286, https://doi.org/10.1038/s41563-019-0535-9.
[11] I. El Azhari, J. Garcia, M. Zamanzade, F. Soldera, C. Pauly, L. Llanes, F. Mücklich, Investigations on micro-mechanical properties of polycrystalline Ti(C,N) and Zr(C,N) coatings, Acta Mater. 149 (2018) 364–376, https://doi.org/10.1016/j.actamat.2018.02.053.
[12] I. El Azhari, J. García, F. Soldera, S. Suarez, E. Jiménez-Piqué, F. Mücklich, L. Llanes, Contact damage investigation of CVD carbonitride hard coatings deposited on cemented carbides, Int. J. Refract. Met. Hard Mater. 86 (2020) 105050, https://doi.org/10.1016/j.ijrmhm.2019.105050.
[13] I. El Azhari, J. García, M. Zamanzade, F. Soldera, C. Pauly, C. Motz, L. Llanes, F. Mücklich, Micromechanical investigations of CVD coated WC-Co cemented carbide by micropillar compression, Mater. Des. 186 (2020) 108283, https://doi.org/10.1016/j.matdes.2019.108283.
[14] M. Moreno, I. El Azhari, D. Apel, M. Meixner, W. Wan, H. Pinto, F. Soldera, F. Mücklich, J. García, Design of comb crack resistant milling inserts: a comparison of stresses, crack propagation, and deformation behavior between Ti(C,N)/α-Al2O3 and Zr(C,N)/α-Al2O3 CVD coatings, Crystals 11 (2021) 493, https://doi.org/10.3390/cryst11050493.
[15] J. García, V. Collado Ciprés, A. Blomqvist, B. Kaplan, Cemented carbide microstructures: a review, Int. J. Refract. Met. Hard Mater. 80 (2019) 40–68, https://doi.org/10.1016/j.ijrmhm.2018.12.004.
[16] V.S. Neshpor, Yu.N. Vil'k, I.N. Danisina, Change in the electro- and thermophysical properties in pseudobinary alloys along the ray ZrC0.92-ZrN0.85 of the zirconium-nitrogen-carbon system, Sov. Powder Metall. Met. Ceram. 6 (1967) 68–71, https://doi.org/10.1007/BF00773386.
[17] V.G. Grebenkina, M.I. Lesnaya, Electro and thermophysical properties of alloys of the ZrC-ZrN system, Sov. Powder Metall. Met. Ceram. 16 (1977) 448–451, https://doi.org/10.1007/BF00790797.
[18] R. Harrison, O. Ridd, D.D. Jayaseelan, W.E. Lee, Thermophysical characterisation of ZrCxNy ceramics fabricated via carbothermic reduction–nitridation, J. Nucl. Mater. 454 (2014) 46–53, https://doi.org/10.1016/j.jnucmat.2014.07.030.
[19] R. Harrison, O. Rapaud, N. Pradeilles, A. Maître, W.E. Lee, On the fabrication of ZrCxNy from ZrO_2 via two-step carbothermic reduction–nitridation, J. Eur. Ceram. Soc. 35 (2015) 1413–1421, https://doi.org/10.1016/j.jeurceramsoc.2014.11.005.
[20] R. Harrison, Processing and Characterisation of ZrCxNy Ceramics as a Function of Stoichiometry via Carbothermic Reduction-Nitridation, (2015). https://doi.org/10.25560/24810.
[21] K. Constant, R. Kieffer, P. Ettmayer, Über das pseudoternäre System "ZrO"-ZrN-ZrC, Mon. Für Chem. 106 (1975) 823–832, https://doi.org/10.1007/BF00900860.
[22] W. Lengauer, Transition Metal Carbides, Nitrides, and Carbonitrides, in: R. Riedel (Ed.), Handb. Ceram. Hard Mater., 1st ed., Wiley, 2000, pp. 202–252, https://doi.org/10.1002/9783527618217.ch7.
[23] J. Kim, Y.J. Suh, Temperature- and pressure-dependent elastic properties, thermal expansion ratios, and minimum thermal conductivities of ZrC, ZrN, and Zr

(C0.5N0.5), Ceram. Int. 43 (2017) 12968–12974, https://doi.org/10.1016/j.ceramint.2017.06.195.
[24] S.V. Ushakov, A. Navrotsky, Q.-J. Hong, A. Van De Walle, Carbides and nitrides of zirconium and hafnium, Materials 12 (2019) 2728, https://doi.org/10.3390/ma12172728.
[25] K. Thompson, D. Lawrence, D.J. Larson, J.D. Olson, T.F. Kelly, B. Gorman, In situ site-specific specimen preparation for atom probe tomography, Ultramicroscopy 107 (2007) 131–139, https://doi.org/10.1016/j.ultramic.2006.06.008.
[26] P.-P. Choi, I. Povstugar, J.-P. Ahn, A. Kostka, D. Raabe, Thermal stability of TiAlN/CrN multilayer coatings studied by atom probe tomography, Ultramicroscopy 111 (2011) 518–523, https://doi.org/10.1016/j.ultramic.2010.11.012.
[27] J. Angseryd, F. Liu, H.-O. Andrén, S.S.A. Gerstl, M. Thuvander, Quantitative APT analysis of Ti(C,N), Ultramicroscopy 111 (2011) 609–614, https://doi.org/10.1016/j.ultramic.2011.01.031.
[28] I. Povstugar, P.-P. Choi, D. Tytko, J.-P. Ahn, D. Raabe, Interface-directed spinodal decomposition in TiAlN/CrN multilayer hard coatings studied by atom probe tomography, Acta Mater. 61 (2013) 7534–7542, https://doi.org/10.1016/j.actamat.2013.08.028.
[29] I.C. Schramm, M.P. Johansson Jõesaar, J. Jensen, F. Mücklich, M. Odén, Impact of nitrogen vacancies on the high temperature behavior of (Ti1−xAlx)Ny alloys, Acta Mater. 119 (2016) 218–228, https://doi.org/10.1016/j.actamat.2016.08.024.
[30] I.C. Schramm, C. Pauly, M.P. Johansson Jõesaar, S. Slawik, S. Suarez, F. Mücklich, M. Odén, Effects of nitrogen vacancies on phase stability and mechanical properties of arc deposited (Ti 0.52 Al 0.48)N y (y < 1) coatings, Surf. Coat. Technol. 330 (2017) 77–86, https://doi.org/10.1016/j.surfcoat.2017.09.043.
[31] I. El Azhari, J. Barrirero, J. García, F. Soldera, L. Llanes, F. Mücklich, Atom Probe Tomography investigations on grain boundary segregation in polycrystalline Ti(C,N) and Zr(C,N) CVD coatings, Scr. Mater. 162 (2019) 335–340, https://doi.org/10.1016/j.scriptamat.2018.11.041.
[32] I.E. Azhari, J. Barrirero, N. Valle, J. García, L. Von Fieandt, M. Engstler, F. Soldera, L. Llanes, F. Mücklich, Impact of temperature on chlorine contamination and segregation for Ti(C,N) CVD thin hard coating studied by nano-SIMS and atom probe tomography, Scr. Mater. 208 (2022) 114321, https://doi.org/10.1016/j.scriptamat.2021.114321.
[33] F. Vogel, S. Ngai, C.J. Smith, R. Holler, C.R. Weinberger, N. Wanderka, G. B. Thompson, Carbide and nitride phase characterization in a transition metal carbo-nitride using x-ray spectroscopy and atom probe tomography, Micron 122 (2019) 32–40, https://doi.org/10.1016/j.micron.2019.04.005.
[34] J. Takahashi, K. Kawakami, Y. Kobayashi, T. Tarui, The first direct observation of hydrogen trapping sites in TiC precipitation-hardening steel through atom probe tomography, Scr. Mater. 63 (2010) 261–264, https://doi.org/10.1016/j.scriptamat.2010.03.012.
[35] J. Webel, A. Herges, D. Britz, E. Detemple, V. Flaxa, H. Mohrbacher, F. Mücklich, Tracing microalloy precipitation in Nb-Ti HSLA steel during austenite conditioning, Metals 10 (2020) 243, https://doi.org/10.3390/met10020243.
[36] J. Webel, L. Weber, E. Vardo, D. Britz, T. Kraus, F. Mücklich, Particle encapsulation techniques for atom probe tomography of precipitates in microalloyed steels, Ultramicroscopy 223 (2021) 113219, https://doi.org/10.1016/j.ultramic.2021.113219.
[37] J. Webel, H. Mohrbacher, E. Detemple, D. Britz, F. Mücklich, Quantitative analysis of mixed niobium-titanium carbonitride solubility in HSLA steels based on atom probe tomography and electrical resistivity measurements, J. Mater. Res. Technol. 18 (2022) 2048–2063, https://doi.org/10.1016/j.jmrt.2022.03.098.
[38] Y. Kobayashi, J. Takahashi, K. Kawakami, K. Hono, Determination of the chemical compositions of fine titanium carbide and niobium carbide precipitates in isothermally aged ferritic steel by atom probe tomography analysis, Microsc. Microanal. 27 (2021) 1–11, https://doi.org/10.1017/S143192762002471X.
[39] L. Weber, J. Webel, F. Mücklich, T. Kraus, Precipitate number density determination in microalloyed steels by complementary atom probe tomography and matrix dissolution, J. Mater. Sci. 57 (2022) 12585–12599, https://doi.org/10.1007/s10853-022-07398-z.
[40] M. Kapoor, R. O'Malley, G.B. Thompson, Atom probe tomography study of multi-microalloyed carbide and carbo-nitride precipitates and the precipitation sequence in Nb-Ti HSLA steels, Metall. Mater. Trans. A 47 (2016) 1984–1995, https://doi.org/10.1007/s11661-016-3398-6.
[41] G.B. Thompson, M.K. Miller, H.L. Fraser, Some aspects of atom probe specimen preparation and analysis of thin film materials, Ultramicroscopy 100 (2004) 25–34, https://doi.org/10.1016/j.ultramic.2004.01.010.
[42] B. Gault, M.P. Moody, J.M. Cairney, S.P. Ringer, Atom Probe Microscopy, Springer New York, New York, NY, 2012, https://doi.org/10.1007/978-1-4614-3436-8.
[43] H.-O. Andrén, A. Henjered, D.R. Kingham, On the charge state of tungsten ions in the pulsed-field atom probe, Surf. Sci. 138 (1984) 227–236, https://doi.org/10.1016/0039-6028(84)90508-9.
[44] U. Rolander, H.-O. Andrén, On atom-probe analysis of cubic MX-type carbides and carbonitrides, C6-299-C6-304, J. Phys. Colloq. 49 (1988), https://doi.org/10.1051/jphyscol:1988652.
[45] H.-O. Andrén, U. Rolander, P. Lindahl, Atom-probe analysis of cemented carbides and cermets, Appl. Surf. Sci. 76–77 (1994) 278–284, https://doi.org/10.1016/0169-4332(94)90355-7.
[46] W. Lengauer, S. Binder, K. Aigner, P. Ettmayer, A. Guillou, J. Debuigne, G. Groboth, Solid state properties of group IVb carbonitrides, J. Alloy. Compd. 217 (1995) 137–147, https://doi.org/10.1016/0925-8388(94)01315-9.
[47] M. Thuvander, J. Weidow, J. Angseryd, L.K.L. Falk, F. Liu, M. Sonestedt, K. Stiller, H.-O. Andrén, Quantitative atom probe analysis of carbides, Ultramicroscopy 111 (2011) 604–608, https://doi.org/10.1016/j.ultramic.2010.12.024.
[48] L. Gribaudo, D. Arias, J. Abriata, The N-Zr (Nitrogen-Zirconium) system, J. Phase Equilibria 15 (1994) 441–449, https://doi.org/10.1007/BF02647575.
[49] X. Ma, C. Li, K. Bai, P. Wu, W. Zhang, Thermodynamic assessment of the Zr–N system, J. Alloy. Compd. 373 (2004) 194–201, https://doi.org/10.1016/j.jallcom.2003.10.051.
[50] M.E. Straumanis, C.A. Faunce, W.J. James, The defect structure and bonding of zirconium nitride containing excess nitrogen, Inorg. Chem. 5 (1966) 2027–2030, https://doi.org/10.1021/ic50045a040.
[51] O.V. Pshenichnaya, M.A. Kuzenkova, P.S. Kislyi, The sintering of zirconium nitride in vacuum and in nitrogen, Sov, Powder Metall. Met. Ceram. 14 (1975) 986–989, https://doi.org/10.1007/BF00807873.
[52] K. Wheeler, P. Peralta, M. Parra, K. McClellan, J. Dunwoody, G. Egeland, Effect of sintering conditions on the microstructure and mechanical properties of ZrN as a surrogate for actinide nitride fuels, J. Nucl. Mater. 366 (2007) 306–316, https://doi.org/10.1016/j.jnucmat.2007.03.023.
[53] N. Alexandre, M. Desmaison-Brut, F. Valin, M. Boncoeur, Mechanical properties of hot isostatically pressed zirconium nitride materials, J. Mater. Sci. 28 (1993) 2385–2390, https://doi.org/10.1007/BF01151669.
[54] A. Fernández Guillermet, Analysis of thermochemical properties and phase stability in the zirconium-carbon system, J. Alloys Compd. 217 (1995) 69–89, https://doi.org/10.1016/0925-8388(94)01310-E.
[55] C. Gasparrini, D. Rana, N. Le Brun, D. Horlait, C.N. Markides, I. Farnan, W.E. Lee, On the stoichiometry of zirconium carbide, Sci. Rep. 10 (2020) 6347, https://doi.org/10.1038/s41598-020-63037-0.
[56] D.B.K. Rana, E.Z. Solvas, W.E. Lee, I. Farnan, An investigation of the long-range and local structure of sub-stoichiometric zirconium carbide sintered at different temperatures, Sci. Rep. 10 (2020) 3096, https://doi.org/10.1038/s41598-020-59698-6.
[57] S. Das, D. Dubois, M.S.I. Sozal, Y. Emirov, B. Jafarizadeh, C. Wang, V. Drozd, A. Durygin, Z. Cheng, Synthesis and flash sintering of zirconium nitride powder, J. Am. Ceram. Soc. 105 (2022) 3925–3936, https://doi.org/10.1111/jace.18421.
[58] Y. Zhang, B. Liu, J. Wang, Self-assembly of Carbon Vacancies in Sub-stoichiometric ZrC1−x, Sci. Rep. 5 (2015) 18098, https://doi.org/10.1038/srep18098.
[59] A.I. Gusev, Effect of nonstoichiometry on anisotropy of elastic properties of disordered cubic zirconium carbide ZrC, Int. J. Refract. Met. Hard Mater. 113 (2023) 106192, https://doi.org/10.1016/j.ijrmhm.2023.106192.
[60] R. Kieffer, F. Benesovsky, Die Karbide, Hartstoffe, Springer Vienna, Vienna, 1963, pp. 44–286, https://doi.org/10.1007/978-3-7091-7151-6_3.
[61] T. Davey, Y. Chen, The effect of oxygen impurities on the stability and structural properties of vacancy-ordered and -disordered ZrC $_x$, RSC Adv. 12 (2022) 3198–3215, https://doi.org/10.1039/D1RA07768F.
[62] F. Réjasse, O. Rapaud, G. Trolliard, O. Masson, A. Maître, Experimental investigation and thermodynamic evaluation of the C–O–Zr ternary system, RSC Adv. 6 (2016) 100122–100135, https://doi.org/10.1039/C6RA21967E.
[63] N.J. Ashley, R.W. Grimes, K.J. McClellan, Accommodation of non-stoichiometry in TiN1-x and ZrN1-x, J. Mater. Sci. 42 (2007) 1884–1889, https://doi.org/10.1007/s10853-006-1321-z.
[64] Y. Tang, G.-J. Zhang, J.-X. Xue, X.-G. Wang, C.-M. Xu, X. Huang, Densification and mechanical properties of hot-pressed ZrN ceramics doped with Zr or Ti, J. Eur. Ceram. Soc. 33 (2013) 1363–1371, https://doi.org/10.1016/j.jeurceramsoc.2012.12.013.
[65] V.A. Mitrokhin, R.A. Lyutikov, R.S. Yurkova, Change in the lattice constant of zirconium carbide in the region of homogeneity, Inorg. Mater. USSR Engl. Transl. V 11 (No 6) (1975) 978–980. ⟨https://www.osti.gov/biblio/4012964⟩.
[66] I.L. Shabalin, Zirconium Monocarbide. Ultra-High Temp. Mater. II, Springer Netherlands, Dordrecht, 2019, pp. 423–675, https://doi.org/10.1007/978-94-024-1302-1_5.
[67] V.I. Ivashchenko, P.E.A. Turchi, V.I. Shevchenko, First-principles study of elastic and stability properties of ZrC–ZrN and ZrC–TiC alloys, J. Phys. Condens. Matter 21 (2009) 395503, https://doi.org/10.1088/0953-8984/21/39/395503.
[68] L. Vegard, Die Konstitution der Mischkristalle und die Raumfüllung der Atome, Z. F. üR. Phys. 5 (1921) 17–26, https://doi.org/10.1007/BF01349680.
[69] A.R. Denton, N.W. Ashcroft, Vegard's law, Phys. Rev. A 43 (1991) 3161–3164, https://doi.org/10.1103/PhysRevA.43.3161.
[70] G. Samsonov, G.S. Upadkhaya, V. Neshpor, Physical materials science of carbides, Kiev. "Nauk. Dumka 456 (1974).
[71] E.K. Storms, The Zirconium–Zirconium Carbide System. in: Refract. Mater., Elsevier, 1967, pp. 18–34, https://doi.org/10.1016/B978-1-4832-3070-2.50007-0.
[72] V.P. Bulychev, R.A. Andrievskii, L.B. Nezhevenko, The sintering of zirconium carbide, Sov. Powder Metall. Met. Ceram. 16 (1977) 273–276, https://doi.org/10.1007/BF00806128.